World Applied Sciences Journal 28 (4): 440-448, 2013
ISSN 1818-4952

DOI: 10.5829/idosi.wasj.2013.28.04.2053

Optimal Operation Management of a Typical Microgrid as Grid Connected in Power Systems Using Fuzzy Sliding-Mode Control (FSMC) Approach

M. Mohammad

Department of Electrical Engineering, Borujerd Branch, Islamic Azad University, Borujerd, Iran

Abstract: This paper presents modeling and control of a hybrid distributed energy sources including photovoltaic (PV), fuel cell (FC) and battery energy storage (BES) in a microgrid which provides both real and reactive power to support a utility grid using fuzzy sliding-mode control (FSMC). The overall configuration of the microgrid including dynamic models for the PV, FC, BES and its power electronic interfacing are briefly described. Then controller design methodologies for the power conditioning units to control the power flow from the hybrid power plant to the utility grid are presented. In order to distribute the power between power sources, the power sharing controller has been developed. Simulation results are presented to demonstrate the effectiveness of the control strategy.

Key words: Microgrid · Power Control · Renewable energy · Fuel Cell · Photovoltaic

INTRODUCTION

Integration of distributed energy resources (DER) units with energy storages has brought about the concept of microgrid [1-3]. A microgrid is defined as a cluster of energy sources include wind turbine, photovoltaic, fuel cell and loads, serviced by a distribution system and can operate in the grid-connected mode, the islanded (autonomous) mode and ride-through between the two modes [4].

Combining the non-dispatchable renewable energy sources, like solar energy with dispatchable energy sources like fuel cell and energy storage make the best use of the advantages of each individual device [5]. Hybridization of fuel cell with PV will therefore form a very reliable distributed generation where the fuel cell acts as back up during low PV output [6]. The energy storage can be used to supply high transient energy and thus greatly improve system dynamics [7]. A microgrid can be strategically placed at any site in a power system (normally at the distribution level) for grid reinforcement, thereby deferring or eliminating the need for system upgrades and improving system integrity, reliability and efficiency. When it is connected to a utility grid, important operation and performance requirements are imposed on microgrid.

The main challenge in operating such hybrid system is the coordination of the numerous generators for sharing the real and reactive power output and the control of system frequency and voltage.

Up to now many studies have been presented for control and management of microgrid. Some of them have concentrated on the operation of control strategies in microgrid [8-10]. In these researches, the modeling of microgrid and implementation of control strategies have not been considered. In other investigations, only the control of power electronic converters in microgrid has been discussed [11-14].

However, in order to power control of microgrid it is necessary to study the whole system with considering the dynamical and physical properties of each power sources in microgrid and the power electronic converters.

Hence, in this paper, power management strategy of a microgrid in grid connected mode is introduced. First, dynamic model of hybrid renewable energy sources in a microgrid is presented.

The hybrid power plant is interfaced with the utility grid via boost dc/dc converters and a three-phase pulsewidth modulation (PWM) inverter. The models for the boost dc/dc converter and the three-phase inverter together are also addressed. The overall aim is to split the active power flow between hybrid power sources and

Corresponding Author: M. Mohammad, Department of Electrical Engineering, Borujerd Branch, Islamic Azad University, Borujerd, Iran.

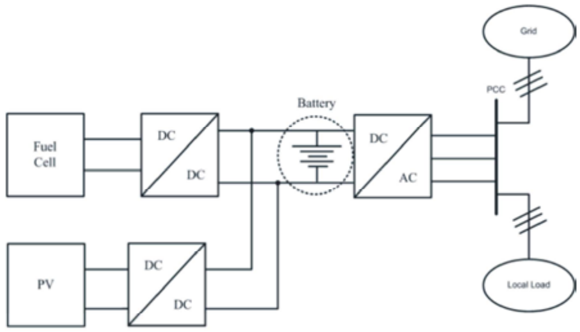

Fig. 1: Hybrid Renewable energy sources in a microgrid

control of active and reactive power of this microgrid while taking into account component and system constraints. A control strategy for reliable power sharing between power sources in the microgrid is proposed and simulation results are shown with real and reactive power control capability.

Proposed Structure of Microgrid Based on Hybrid Renewable Power Sources: The dynamic modeling of Hybrid Renewable Power Sources (HRPS) system is an important issue that needs to be carefully addressed. To study the performance characteristics of HRPS systems, accurate models of fuel cell, photovoltaic and battery energy storage are needed. Moreover, models for the interfacing power electronic circuits in a HRPS system are also needed to design controllers for the overall system to improve its performance and to meet certain operation requirements. To meet the system operational requirements, a HRPS system needs to be interfaced through a set of power electronic devices. Fig.1 shows the block diagram of the HRPS proposed in this paper that connected to main grid in Point Common Coupling (PCC). The mathematical models describing the dynamic behavior of each of these components are given below.

Fuel Cell Model: Fuel cells are static energy conversion devices that convert the chemical energy of fuel directly into electrical energy. The model of fuel cell power plant used in this study is based on the dynamic PEMFC stack model developed in [16]. The performance of fuel cell is affected by several operating variables, as discussed in the following. This model is based on simulating the relationship between output voltage and partial pressure of hydrogen, oxygen and water. The Nernst's equation and Ohm's law determine the average voltage magnitude of the fuel cell stack. The following equation shows the voltage of the fuel cell stack:

$$V_{fc} = N_0(E_0 + \frac{RT}{2F}(\log(\frac{P_{H_2}P_{O_2}^{0.5}}{P_{H_2O}})) - R_{\text{int}}I \quad (1)$$

Where:

- N_0 is the number of cells connected in series;
- R_{int} is the internal resistance of fuel cell stack [Ω]
- E_0 is the voltage associated with the reaction free energy;
- R is the universal gas constant;
- T is the temperature;
- I is the current of the fuel cell stack;
- F is the Faraday's constant.
- P_{H2}, P_{H2O}, P_{O2} are determined by the following differential equations:

$$\dot{P}_{H_2} = -\frac{1}{t_{H_2}}(P_{H_2} + \frac{1}{K_{H_2}}(q_{H_2}^{in} - 2K_rI_{fc}))$$

$$\dot{P}_{H_2O} = -\frac{1}{t_{H_2O}}(P_{H_2O} + \frac{2}{K_{H_2O}}K_rI_{fc})) \quad (2)$$

$$\dot{P}_{O_2} = -\frac{1}{t_{O_2}}(P_{O_2} + \frac{1}{K_{O_2}}(q_{O_2}^{in} - K_rI_{fc}))$$

Where, $q_{H_2}^{in}$ and $q_{O_2}^{in}$ are the molar flow of hydrogen and oxygen and where the K_r constant is defined by the relation between the rate of reactant hydrogen and the fuel cell current:

$$q_{H_2}^{r} = \frac{N_0I}{2F} = 2K_rI \quad (3)$$

Moreover, a simple model of reformer that generates hydrogen through methane has been considered. The model is second-order transfer function. The mathematical form of the model can be written as follows:

$$\frac{q_{H_2}}{q_{methane}} = \frac{CV}{\tau_1\tau_2s^2 + (\tau_1 + \tau_2)s + 1} \quad (4)$$

Where

$q_{methane}$ is methane flow rate [kmol/sec];
CV is conversion factor [kmol of hydrogen per kmol of methane];
τ_1, τ_2 are reformer time constants [sec].

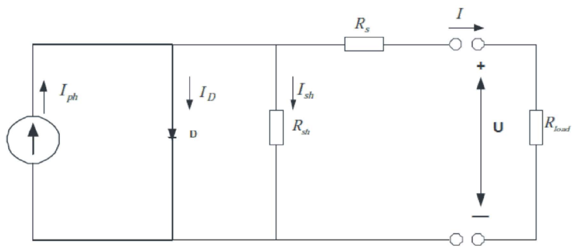

Fig. 2: One diode model of PV

Photovoltaic Model: The photovoltaic arrays (PVs) are an attractive source of renewable energy for distributed urban power generation due to their relatively small size and noiseless operation. Their applications are expected to significantly increase all over the world. The most common PV model used is the one diode model. The model used in this paper is the one diode model whose equivalent circuit is shown in Fig.2. An initial understanding of the performance of a solar cell may be obtained by considering it as a diode. The light energy, which is in the form of photons with the appropriate energy level, falls on the cell and generates electron-hole pairs. The electrons and holes are separated by the electric field established at the junction of the diode and are then driven around an external circuit by this junction potential [17].

The PV cell can be modeled as a diode in parallel with a constant current source and a shunt resistor. These three components are in series with the series resistor. The output terminal current I is equal to the light-generated current I_{ph}, with subtracted diode current I_D and the shunt-leakage current I_{sh}.

$$I = I_{ph} - I_D - I_{sh} \tag{5}$$

The series resistance Rs represents the internal resistance of the current flow and it depends on the p-n junction depth, the impurities and the contact resistance. The shunt resistance R_{sh} is inversely related to the leakage current to the ground. In an ideal PV cell, $Rs = 0$ (no series loss) and $R_{sh} = 1$ (no leakage to ground). The PV cell conversion efficiency is sensitive to small variations in R_s, but is insensitive to variations in R_{sh}. A small increase in R_s can decrease the PV output significantly. In the equivalent circuit, the current delivered to the external load equals the current I_{ph} generated by the illumination, less than the diode current I_D and the ground-shunt current I_{sh}. The open circuit voltage U_{oc} of the cell is obtained when the load current is zero, i.e. when $I_{sh} = 0$ and is given as:

$$U_{OC} = U + IR_S \tag{6}$$

Where, U is the terminal voltage of the cell [V].

The diode current I_D is given by the classical diode current expression [18]:

$$I_D = I_d\left[\frac{qU_{oc}}{A_c f K_B T} - 1\right] \tag{7}$$

Where

- I_d is the saturation current of the diode,
- q is electron charge = 1.6×10^{-19} Coulombs,
- A_{cf} is curve fitting constant,
- K_B is Boltzmann constant = 1.38×10^{-23} Joule/ °KT
- T is temperature [°K].

$$I = I_{ph} - I_{OS}\left\{\exp\left[\frac{qU_{OC}}{A_C f K_B T}\right] - 1\right\} - \frac{U_{OC}}{R_{sh}} \tag{8}$$

The output current is given by [18]:

Where:

$$I_{ph} = \frac{G}{100}\left[I_{SCR} + K_I(T - 25)\right] \tag{9}$$

$$I_{oc} = I_{o\gamma}\left(\frac{T}{T_\gamma}\right)^3 \exp\left[\frac{qE_{GO}}{BK_B}\left(\frac{1}{T_\gamma} - \frac{1}{T}\right)\right] \tag{10}$$

Where

I, U	=	Cell output current and voltage,
I_{os}	=	Cell reverse saturation current,
B	=	Ideality factor of p-n junction,
K_I	=	Short circuit current temperature coefficient at I_{SCR}, K_I= 0.0017 A/°C,
G	=	Solar irradiation in W/m^2,
I_{SCR}	=	short circuit current at 25°C and 1000W/m2,
I_{ph}	=	Light generated current
E_{GO}	=	Band gap for silicon,
T_r	=	Reference temperature, T_r=301.18°K,
I_{or}	=	Cell saturation current at T_r,
R_{sh}	=	Shunt resistance,
R_s	=	Series resistance.
I_{SCR}	=	The current at maximum power point (I_{mpp}), the voltage at maximum power point (V_{mpp}) and the open circuit voltage of the cell U_{oc}, are given by the manufacturers.

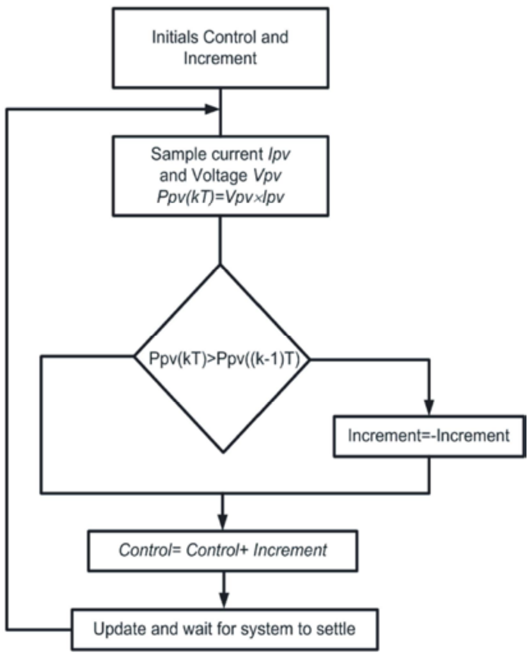

Fig. 3: Perturb and observe algorithm for MPPT

The photovoltaic module operates at on the V-I characteristics that are determined by the load. Since the power harvested from the photovoltaic module is different at different operating points it is important that the load is matched in such a way that maximum power is obtained from the photovoltaic module [19]. The simplest and widely known algorithm is the "perturb and observe" algorithm. It works by periodically ching the array terminal voltage and comparing the calculated power with that from the previous samples as shown in Fig. 3.

There are other numerous and more complex and efficient algorithms and a comparative study has been done on these algorithms [20].

Boost DC/DC Converter Model: The role of boost DC/DC converters is to provide power to the user in a suitable form at high efficiency. Power electronic converters are needed in PV and fuel cell systems to convert DC voltage to the required values. Fig.4 shows the DC/DC converter model.

This boost converter is described by the following two non-linear state space averaged equations [21]:

$$\frac{di_L}{dt} = -\frac{R_L}{L} - (\frac{1-d}{L})V_o + \frac{1}{L}V_s$$
$$\frac{dV_C}{dt} = \frac{(1-d)}{C}.i_L - \frac{i_R}{C} \tag{11}$$

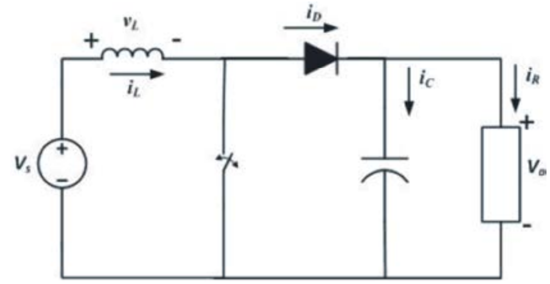

Fig. 4: Boost DC/DC Converter Model

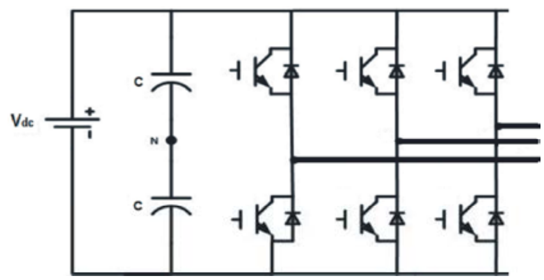

Fig. 5: Three-phase dc/ac voltage source inverter

Where ''d'' is the duty cycle of the switching device, ''U'' is the input voltage, ''i_L'' is the inductor current, ''V_C'' is the output voltage and "i_O" is the output current.

DC-AC Source Converter Model: A three-phase equivalent circuit of DC/AC converter is shown in Fig. 5. A first-order filter, represented by the L_s and the R_s is used to reduce the harmonics in the output voltage of converter. In Fig.5, v_{ia}, v_{ib} and v_{ic} are the three-phase AC voltage outputs of the inverter and i_a, i_b, i_c are the three-phase AC current outputs of the inverter. The bus voltages of the AC system are v_{sa}, v_{sb} and v_{sc}. The dynamic model of the three-phase VSC is represented in [5].

$$\frac{di_k}{dt} = -\frac{R_s}{L_s}i_k + \frac{1}{L_s}(v_{ik} - v_{sk}) \tag{12}$$

Where k= {a, b, c}.

In Park's d-q frame that rotates synchronously with the AC system angular speedω, current dynamics can be reasonably represented by the following equations:

$$v_{iq} = R_s i_q + L_s\frac{di_q}{dt} + L_s\omega i_d + v_{sq}$$
$$v_{id} = R_s i_d + L_s\frac{di_d}{dt} - L_s\omega i_q + v_{sd} \tag{13}$$

where v_{id}, v_{iq}, i_d, i_q are the d-and q- axis inverter's voltages and currents and v_{sd}, v_{sq} are the d- and q- axis components of the supply voltage at the PCC.

Power Flow Control: Power flow control from hybrid power sources to local AC bus and to/from storage devices is required to maintain power balance at all times while satisfying the active and reactive power demanded by the load. Equation (14) gives power balance expressions that should be satisfied both at the DC-link and at the PCC at all times. The rate and magnitude of fuel cell power P_{FC} and rate, sign and magnitude of battery power P_{Batt} depend on the magnitude and how fast the load changes.

$$\begin{aligned} P_{MG} &= P_{PV} + P_{FC} + P_{Batt} \\ P_{Load} &= P_{MG} + P_{Grid} \\ Q_{Load} &= Q_{MG} + Q_{Grid} \end{aligned} \qquad (14)$$

According to the control strategy proposed in this paper, P_{Load} and Q_{Load} are made equal to P_{ref} and Q_{ref} so that the hybrid power system output follows the load demand under normal loading conditions and P_{Grid} and Q_{Grid} are zero. If the local load demand exceeds the hybrid power system capacity, the rest of the power is supplied from the grid. The control strategy also keeps the DC-link/battery voltage within a band around the nominal DC-link voltage to keep the inverter in synchronism with the grid. Fig.6 shows the overall structure of the control strategy. More detailed control strategies of each component follows in the subsequent subsections.

Control of PV Subsystem: To fully utilize the renewable energy from the PV source, it is always operated at the maximum power point. The output of the PV source in this system can be considered uncontrolled and is a priority source in terms of which source to use first. Below are three scenarios that are used and control strategies imparted for each case:

PV Output is Equal to Power Demanded by Local Load: Here only PV energy is used except during transients when the battery may come in. Fuel Cell output should be effectively zero to save power.

PV Output is less than Power Demanded by the Local Load: If PV is not able to meet the load demand, the rest of demand is compensated from the fuel cell source. In case demand minus PV power is bigger than the fuel cell capacity, both fuel cell and battery will meet the deficit.

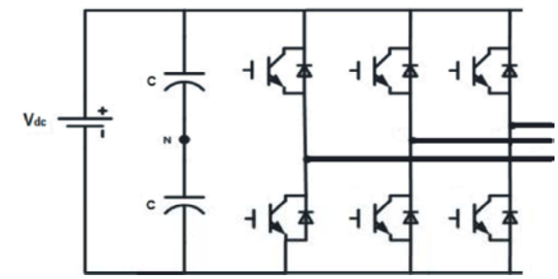

Fig. 6: Overall system control structure

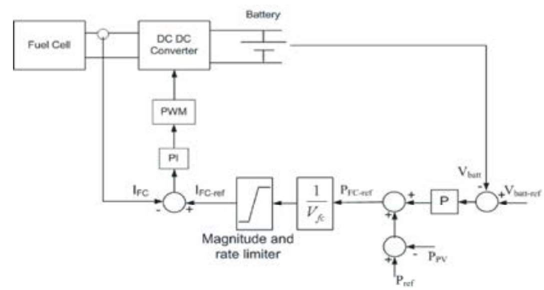

Fig. 7: Control of fuel cell subsystem

PV Output is Greater than Power Demanded by the Local Load: Any excess PV than is required by the load goes to charging the battery. If the remaining PV power is more than required to charging the battery, this may overcharge it. This excess energy should therefore be dumped into a dump load.

Control of Fuel Cell Subsystem: The fuel cell reference power is generated as the difference between the load power demanded minus the PV power. An additional power proportional to the difference of battery reference voltage and the current battery voltage is generated by an outer loop voltage controller to charge the battery. This additional power is then added to the fuel cell reference power demanded from the load to generate the overall fuel cell power reference. A proportional controller is sufficient for batteries with flat voltage profiles as in Li-ion battery. Fig.7 shows the control strategy of the fuel cell subsystem.

To directly modulate the fuel cell DC/DC converter an internal PI current controller is implemented. This controller takes the fuel cell current reference and generates appropriate control voltage to the PWM which ultimately controls the boost converter. The fuel cell current reference is limited both in magnitude and rate to allow the fuel cell operate at steady state and within safe operating region and below the reactant concentration current. The limiter allows the battery to respond to fast changing load power demands.

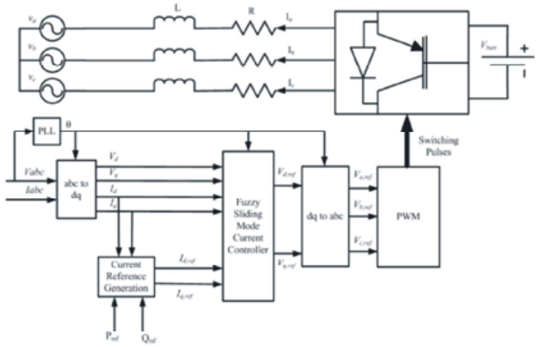

Fig. 8: Control structure of three phase inverter

Control of Grid Connected Inverter: The voltage source inverter is controlled to transfer the reference real and reactive powers P_{ref} and Q_{ref} demanded by the load. The reference powers are used to generate reference currents $i_{d,ref}$ and $i_{q,ref}$ in the *dq* reference frame as given in (15). The three phase grid currents and voltages are measured and transformed into *dq*-components. Then they are used along with the reference current signals in the current control algorithm to produce the reference voltage signals for the PWM regulator as shown in Fig.8.

$$\begin{bmatrix} i_{d,ref} \\ i_{q,ref} \end{bmatrix} = \begin{bmatrix} v_d & v_q \\ v_q & -v_d \end{bmatrix}^{-1} \begin{bmatrix} P_{ref} \\ Q_{ref} \end{bmatrix} \tag{15}$$

The phase locked loop (PLL) estimates the grid voltage phase angle which is then used to synchronize the inverter output voltage to the grid.

According to the control strategy, the purpose of the current controller is to synthesize a voltage correction vector that keeps the current error vector to a minimum value. The error current-vector is defined in (16)

$$\begin{bmatrix} \Delta i_d \\ \Delta i_q \end{bmatrix} = \begin{bmatrix} i_{d,ref} \\ i_{q,ref} \end{bmatrix} - \begin{bmatrix} i_d \\ i_q \end{bmatrix} \tag{16}$$

where $i_{d,ref}$ and $i_{q,,ref}$ are the reference current commands and i_d and i_q are the measured current feedback all in the *dq*-reference frame.

In this paper, the current controller has been implemented by using fuzzy sliding mode control (FSMC) technique due to its robustness and overshoot-free fast tracking capability.

The sliding-mode control approach is one of the robust control methods to handle systems with model uncertainties. Systematic design procedures for sliding-mode controllers are well known and available in the literature [22]. However, it may result in chattering phenomenon due to the high frequency switching near the sliding surface. The switching-type control law should be avoided in many applications, such as servo control systems and structure vibration control systems and it is hard to achieve in practice. Several methods were proposed to overcome this side effect. The fuzzy sliding-mode control (FSMC) approach is proposed such that it can be applied with advantages to both fuzzy and sliding-mode controller. The structure FSMC is simple and will not result in the chattering phenomena. The FSMC is a hybrid controller and inherits the advantages of fuzzy and sliding-mode controllers. The main advantage of the fuzzy controller is its heuristic design procedure and it is a model-free approach. However, when the fuzzy variables are more than two, the synthesis of a complete fuzzy rule set is not easy. The sliding mode control approach guarantees the robustness and stability of the resulting control system, which can systematically be achieved at the cost of the chattering side effect. The combination of fuzzy control strategy and sliding-mode control method becomes a feasible approach to preserve the advantages of these two approaches. The structure of fuzzy sliding-mode controller is described as follows. Let $s(x) = 0$ be the sliding surface that is determined by design requirements and x is the error state vector. Let s denote the fuzzy variable of the universe of discourse s. Then, some linguistic terms can be defined to describe the fuzzy variable s, such as zero, positive large, or negative smaller, etc. Each linguistic term expresses a certain situation in the system. For example, s is "zero" means the state of system is on the sliding surface or is near to the sliding surface. s is "positive large" means the system state is far from the sliding surface and $s(x) > 0$. Such linguistic expression can be used to form fuzzy control rules as below.

RI: If s is NB then u is PB.
R2: If s is NM then u is PM.
R3: If s is ZO then u is ZO.
R4: If s is PM then u is NM.
R5: If s is PB then u is NB.

where u denotes the fuzzy variable of the universe of discourse of the control signal u, NB denotes *"Negative Big"*, NM denotes *"Negative Mid"*, ZO denotes *"Zero"*, PM denotes *"Positive Mid"* and PB denotes *"Positive Big"*.

RESULTS

To evaluate the effectiveness of the proposed control strategy, the system is simulated in Simulink/simpower over a 100sec of real and reactive load profiles.

The choice of the DC-bus voltage depends on the output voltage of the inverter required which should give the grid voltage. The relationship between the DC link voltage V_{dc} and the line-to-line RMS grid voltage $V_{LL,AC}$, where m_a is the modulation index in the linear region, is given in (17) [23].

$$V_{dc} \geq \frac{1.633}{m_a} V_{LL,AC} + voltagedrops \quad (17)$$

Assuming filter impedance drop of 5% of grid voltage and to give an output voltage of 400V at PCC, the nominal DC-link voltage was chosen at 720V.

Seven strings of each 16 series modules are used to provide a PV peak capacity of around 25kWp. The PV modules are the same as the one modeled in section 2. To test how the control strategy reacts for a varying PV output profile, the irradiance over 300sec was assumed to have variation.

Twenty one 1.2kW, 12-21V PEMFC stacks which are the same as the one modeled in section 2 were stacked in series to provide 25kW power at rated operation. This provides a full back up to the PV during zero PV output. At rated operation the fuel cell stack voltage at the input to the boost converter is 21x12V=252V.

A 11Ah Li-ion battery bank stacked out of the same cells modeled in section 2 is used to form the DC-link. This battery bank has a full charge voltage of around 726V and a 50% SOC voltage of 710V. This voltage band is sufficiently within the inverter operating area. The flat voltage profile of the battery bank is controlled from the DC side as explained in *3*.

Figs. 9 and 10 show the active and reactive load powers and the power delivered from the hybrid power and the grid. Both show that balance of power is satisfied. All the reactive power demand is supplied locally from the hybrid power system enabling the grid to operate at unity power factor. From 50 to 200sec, where the capacity of the hybrid power system is exceeded, the remaining 10kW of the active power is supplemented by the grid. For the rest of the profile where the load is less than or equal to 40kW, all the demand is covered by the hybrid power system.

Figs. 11 and 12 give the microgrid power tracking performance of the inverter controller.

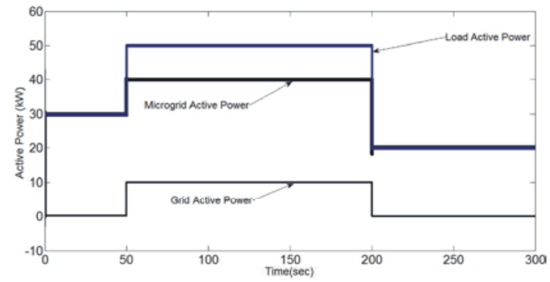

Fig. 9: Active load, microgrid and grid power

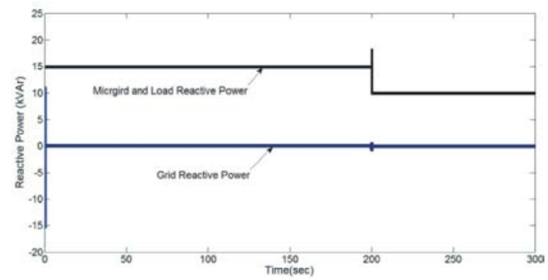

Fig. 10: Reactive load, microgrid and grid power

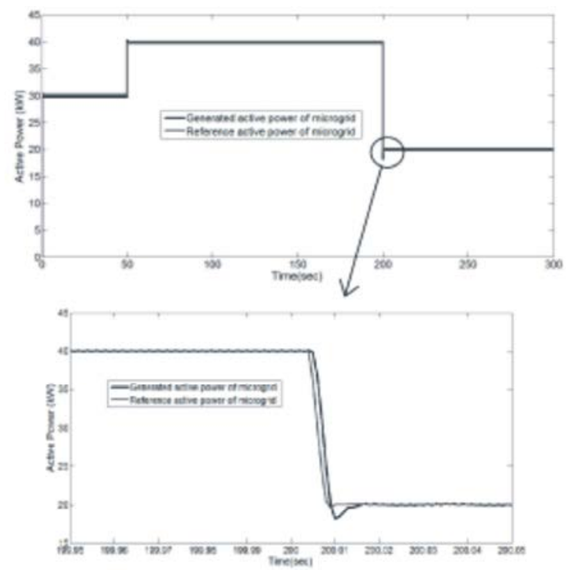

Fig. 11: Generated and reference active power of Microgrid

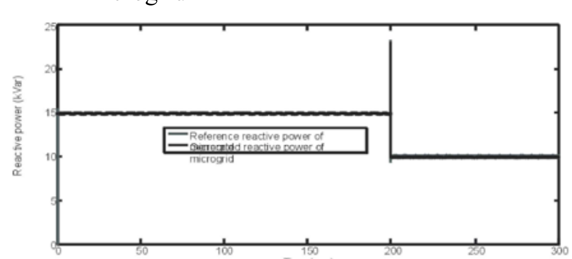

Fig. 12: Generated and reference reactive power of Microgrid

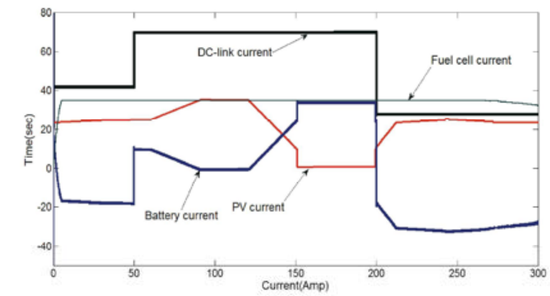

Fig.13: DC-link, PV, Fuel cell and Battery Current

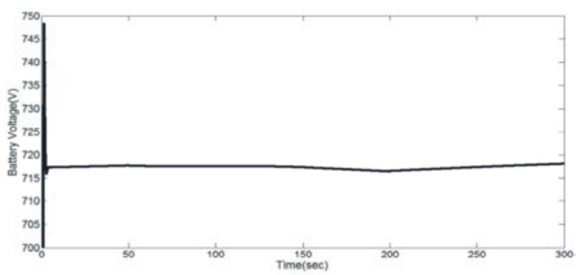

Fig. 14: Battery Voltage

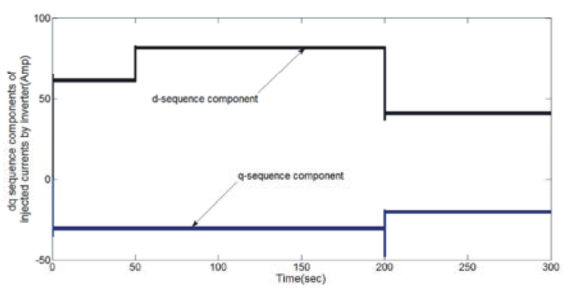

Fig. 15: dq sequence components of injected currents by inverter

It is seen that the controller quickly tracks the reference powers with only small overshoot.

Fig.13 shows the load current sharing between the different power sources and energy storage all referred to the DC-link. Initially, the load active power is supplied from the PV and the fuel cell. Since the initial battery state of charge is 75%, the fuel cell controller requests additional charging power to the battery depending on the difference between the DC-link reference voltage and the battery voltage. At t=50sec, the active load power suddenly increases from 20kW to 50kW and stays for the next 200seconds. At first the battery responds to the instant transient by quickly decreasing its charging current while the fuel cell steadily goes to its maximum output (25kW). Since the maximum capacity (including the battery peak shaving capacity) is only 40kW, the rest 10kW of load power is provided by the grid. From 150 to 200sec, the PV output is very low and the rest of the 40kW microgrid power is provided by the battery. After 200s the PV output increases and the battery current decreases going to charging mode eventually. Starting from 250sec, the fuel cell begins to save fuel and decreases its output since the battery goes to full charge reference voltage of 720V.

Fig.14 shows the battery voltage during the whole power profile. As shown, the power flow control strategy on the DC side always keeps the DC-link voltage within the reasonable range for the inverter.

Fig.15 shows the *dq* sequence components of the injected currents by the inverter. As shown, the fast action of the proposed controller in supplying the power to the grid is obvious.

CONCLUSION

This paper presents modeling, control and power control in a grid connected PV/Fuel Cell/Battery hybrid power generation system in a microgrid. SIMULINK/ SIMPOWER was used to model the system and simulate a power flow control strategy. PV, fuel cell and battery subsystems with power electronic converters are modeled. Then control strategies are designed for power electronic converters based on the classic and fuzzy - sliding mode control. It was shown that the microgrid can be controlled as desired to follow the local demand and allow the grid to operate at or near unity power factor. To distribute the power between power sources, the power sharing controller has been developed. Simulation results are presented to demonstrate the effectiveness of the control strategy.

REFERENCES

1. Lasseter, R.H., 2002. "MicroGrids" in Proc.IEEE Power Engineering Society Winter Meeting, 1: 305-308.
2. Davis, M.W., 2001. "Distributed resource electric power systems offer significant advantages over central station generation and T&D power systems, part I," in IEEE T&D Conference and Exposition, Atlanta, Georgia, Oct./Nov. pp: 54-61.
3. Lasseter, R.H. and P. Piagi, 2004. "MicroGrid: A conceptual solution", in Proc. Power Electronics Specialists Conference, Aachen, Germany, 6: 4285-4290.
4. Katiraei, F. and M.R. Iravani, 2005. "Transients of a Micro-Grid System with Multiple Distributed Energy Resources", International Conference on Power Systems Transients (IPST'05) in Montreal, Canada on, pp: 19-23.

5. Amin Hajizadeh, Masoud Aliakbar Golkar, "Intelligent Power Management Strategy of hybrid Distributed Generation System", International Journal of Electrical Power and Energy Systems, 29: 783-795.
6. Habeebullah H., Saita and S. Arul Daniel, 2001. "New control paradigm for integration of photovoltaic energy sources with utility network", International Journal of Electrical Power & Energy Systems, 33: 86-93.
7. Amin Hajizadeh and Masoud Aliakbar Golkar, 2010. "Control of Hybrid Fuel Cell/Energy Storage Distributed Generation System against Voltage Sag", International Journal of Electric Power and Energy Systems, 32: 488-497.
8. Ramon Zamora and Anurag K. Srivastava, 2010. "Controls for microgrids with storage: Review, challenges and research needs", Renewable and Sustainable Energy Reviews, ELSEVIER,
9. Ali Mehrizi-Sani and Reza Iravani, 2010. "Potential-Function Based Control of a Microgrid in Islanded and Grid-Connected Modes", IEEE Transactions on Power Systems.
10. Joseba Jimeno, Jon Anduaga, Jose´ Oyarzabal and Asier Gil de Muro, 2010. "Architecture of a microgrid energy management system", European Transactions on Electrical Power.
11. Milan Prodanovic and Timothy C. Green, 2003. "Control and Filter Design of Three-Phase Inverters for High Power Quality Grid Connection", IEEE Transactions on Power Electronics, 18(1).
12. Green, T.C. and M. Prodanovic, 2006. "Control of inverter-based micro-grids", Electric Power Systems Research.
13. Milan Prodanovic and Timothy C. Green,"High-Quality Power Generation Through Distributed Control of a Power Park Microgrid", IEEE Transactions on Industrial Electronics, 53(5).
14. Yunwei Li, D., Mahinda Vilathgamuwa and Poh Chiang Loh, 2005. "Microgrid Power Quality Enhancement Using a Three-Phase Four-Wire Grid-Interfacing Compensator", IEEE Transactions on Industry Applications, 41: 6.
15. Yunwei Li, ,D. Mahinda Vilathgamuwa, Poh Chiang Loh," 2006. A Grid-Interfacing Power Quality Compensator for Three-Phase Three-Wire Microgrid Applications", IEEE Transactions on Power Electronics, 21: 4.
16. El-Sharkh, M.Y., A. Rahman, M.Y. Alam, P.C. Byrne, A.A. Sakla and T. Thomas, 2004. "A dynamic model for a stand-alone PEM fuel cell power plant for residential applications", Journal of Power Sources, 138: 199-204.
17. Gow, C.M.J.A., 1999. Development of a photovoltaic array model for use in power-electronics simulation studies," in Electric Power Applications, IEE Proceedings, 146: 193-200.
18. Ishengoma, M.F. and E.E. Norum, 2002. Design and implementation of a digitally controlled stand-alone photovoltaic power supply. In Nordic Workshop on Power and Industrial Electronics (Norpie 2002), Stockholm, Sweden, pp: 12-14.
19. Hussein, K., I. Muta, T. Hoshino and M. Osakada, 1995. "Maximum photovoltaic power tracking: an algorithm for rapidly changing atmospheric conditions", Generation, Transmission and Distribution, IEE Proceedings. 142: 59.
20. Hohm, D. and M. Ropp, 2000. "Comparative study of maximum power point tracking algorithms using an experimental, programmable, maximum power point tracking test bed" Photovoltaic Specialists Conference, 2000. Conference Record of the Twenty-Eighth IEEE, pp: 1699-1702.
21. Yuri, B., Y.B. Shtessel, A. Zinober and A. Shkolnikov," 2005. Sliding mode control of boost and buck-boost power converters using method of stable system centre", Automatica, 39: 1061-1067.
22. Slotine, J.J. and W. Li, 1991. Applied Nonlinear Control (Prentice-Hall, Englewood Cliffs, NJ, 1991.
23. Mohan, N., T.M. Undeland and W.P. Robbins, 2003. Power Electronics Converters,Applications and Design Wiley, 2003.